Dynamics of a penta-hepta defect in a hexagonal pattern

Tammy Tam, Darrick Ohata, Mingming Wu

Department of Physics, Occidental College, Los Angeles, CA 90041, USA

(August 29, 1999)

Abstract

The structure and dynamics of a penta-hepta defect in a hexagonal pattern are studied experimentally. The hexagonal pattern is formed by placing a layer of soap bubbles (diameter ∼1mm) on a flat glass plate. We find that an isolated penta-hepta defect in a bubble raft with free boundary always moves along the direction perpendicular to the wavevector of the nonsingular mode and towards the nearest boundary. The structure of the penta-hepta defect is found to be similar to that found in nonequilibrium pattern forming systems.

PACS numbers: 47.54.+r, 61.72.-y, 47.55.Dz

This Letter describes experimental investigations on the structure and dynamics of an isolated penta-hepta defect in a hexagonal pattern formed by a layer of equal sized (diameter $\sim 1mm$) soap bubbles. Soap bubbles of a certain size range are known to 'crystallize' spontaneously on a flat surface and form a perfect hexagonal pattern [1]. Previous experimental and theoretical work has demonstrated that such a soap bubble raft possesses much of the properties of 2D crystalline systems [1–3]. It is shown that the interactions between the neighboring bubbles can be described by a van der Waals or capillary attraction and a short-range or 'overlap' repulsion [3]. The resulting potential-distance curve reaches a minimum when the distance between the two neighboring bubbles equals to the diameter of the bubble. In other words, the hexagonal lattice formed by the soap bubbles corresponds to the minimum energy state. Several experiments have demonstrated that the properties of dislocations, grain boundaries, stress-strain curves that are typical to a 2D crystalline system exist in the soap bubble raft [1,3].

Recently, much attention has been paid to the structure and dynamics of defects in pattern forming systems far from equilibrium, specifically in Rayleigh-Bénard convections [4–13]. It is found that defects play important roles in the wavevector selection of these systems. The most commonly occurred defect in a 2D hexagonal pattern is the penta-hepta defect(PHD), where a pair of a pentagonal and a heptagonal cell in stead of two neighboring hexagonal cells is observed. Experimental [5,6] and theoretical [10] work on the structure of the PHD has revealed that a PHD requires that two of the three superimposed roll patterns of the hexagonal pattern have dislocations with opposite phase winding numbers. Later observations of the motion of the PHDs in a Rayleigh-Bénard convection [7,8] have inspired a series of theoretical work on the dynamics of the PHDs using the three coupled Ginzburg-Landau equations [11–13]. The mobility of an isolated PHD in a non-optimal wavevector hexagonal pattern is calculated and the interactions of two PHDs are considered. To author's knowledge, these theoretical predictions have not yet been verified by experiments.

It needs to be noted that the hexagonal patterns formed by soap bubbles belong to an *equilibrium* system, while those observed in Rayleigh-Bénard convection belong to an *nonequilibrium* system. However, both systems are potential systems [3,10]. We hope that results presented here will provide insights for the studies of the motion of defects in nonequilibrium systems. Further more, it will stimulate theoretical work on the structure and dynamics of defects in 2D crystalline systems.

The experiment requires a very simple laboratory setup. The soap bubbles are generated by a hypodermic needle submerged in a soap solution. The needle is connected to a constant pressure head provided by an assembly of a pressure needle valve, a pressure regulator and a compressed nitrogen gas tank. The size of the nitrogen filled soap bubbles is adjusted by the needle size and the pressure of the nitrogen. A typical soap solution consists of 28% by weight doubly deionized and doubly distilled water, 44 % regent grade glycerine and 28% Miracle Bubbles (Imperial Toy Corporation, Los Angeles). The bubbles first float on the surface of the soap solution and form naturally a perfect hexagonal pattern. They are then transferred to a flat glass plate with a plastic spoon. Each transfer contains about a dozen bubbles and a small amount of solution. When the bubbles of the first transfer is placed on the glass plate, it forms a perfect hexagonal patch naturally. At each subsequent transfer, the bubbles are added carefully to the edges of the perfect hexagonal patch and the 2D 'crystal' grows spontaneously. Two different boundary conditions are used in our experiments, one is bounded with a $5.41cm$ diameter plastic ring (Fig. 1(a)) and the other is without boundary(Fig. 1(b)). Defects can be seen close to the boundary in the bubble raft with boundary. In the free boundary case, the entire bubble raft is free of defects. The bubbles are very uniform in size, as can be seen by the regularity of the bubble raft in Fig. 1. The hexagonal pattern shown in Fig. 1 is a stable state, it will stay motionless for about an hour. If the raft is left for more than an hour, the bubble size shrinks due to the gas diffusion through the wall. In this case, a viod will appear in the cell near the boundary.

Since soap bubbles form a perfect hexagonal pattern spontaneouly, it is thus necessary for us to introduce PHDs into the system for the study of defect motion. The procedure for introducing a single defect is as follows. First, a perfect hexagonal patch is made as shown in Fig. 1. Second, the perfect hexagonal pattern is raked by a wet needle. Multiple defects are created simultaneously, among which most of them are PHDs. Third, a single PHD near the center of the cell is isolated by getting rid of the unwanted defects. This is usually done by releasing the stress around the unwanted defects using a wet needle. Occasionally, a single PHD can be created by merging two line defects. Very often, we end up with a perfect hexagonal pattern again and the whole process needs to be repeated. In the free boundary case (Fig. 1(b)), the isolated PHD is not a stable state, it moves immediately to its nearest boundary once it is created. This demonstrates that the bubble raft without constrain prefers to stay at its lowest energy state, which is the perfect hexagonal pattern [3]. In the rigid boundary case (Fig. 1(a)), the isolated PHD near the center of the cell is often motionless at the beginning and eventually moves to the boundary. In one case, the motion of the defect is caused by the interactions of the isolated defect near the center with the defects near the boundary. The consequent motion of the isolated PHD is often complicated by the radom distribution of the defects around the boundary. In the other case, a void is formed after a few hours of waiting due to the bubble size shrinkage, and then the defect always choose to move towards the void in a similar way as it does in a cell with free boundary. It moves along the direction perpendicular to the wavevector of nonsigular mode. In the following, we focus on the study of motion of a single defect in a hexagonal pattern with *free boundary*. The motion of multi-defects and the interactions of defects will be the subject of a later publication.

Images of the entire cell are recorded using a SVHS recorder (JVC, BRS822DXU) for the study of the motion of the defect. A time series of $30-60$ images that cover the central portion of the cell is digitized from the video tape at a later time for further data analysis. The two consecutive images are $1s$. apart/ Fig. 2(a) is a typical image of an isolated PHD. It consists of 256(pixel) $\times$ 256(pixel), which corresponds to a viewing area of 2.13(cm) $\times$ 2.13(cm). The bubble size is 0.108cm. The pair of pentagonal and heptagonal cells are marked with two white bars in Fig. 2(a). Fig. 2(b) is the graycale rendition of the modulus $|A(\mathbf{k})|^2$of the Fourier transform of $A(\mathbf{x})$, where $A(\mathbf{x})$ is the gray scale of the hexagonal pattern shown in Fig. 2(a). The six dots indicate the locations of the wavevectors $\pm\mathbf{k_1}$, $\pm\mathbf{k_2}$, $\pm\mathbf{k_3}$

of the three superimposed roll patterns. $\mathbf{k_1}$, $\mathbf{k_2}$ and $\mathbf{k_3}$ are oriented 120^o with respect to each other counter clockwise, a convention used in previous publications [5,13]. Defects can be seen more clearly in two of the three superimposed roll patterns (Fig. 2(c2,c3)). Each roll pattern here is reconstructed by performing inverse fourier transform of $A(\mathbf{k})$ using one pair of peaks. For instance, Fig. 2(c1) is obtained by doing inverse Fourier transform of $A(\mathbf{k})$ after one pair of peaks of $A(\mathbf{k})$ at locations $\pm\mathbf{k_1}$ are singled out using tanh windows [14]. The roll pattern with wavevectors $\pm\mathbf{k_1}$ is defect free (Fig. 2(c1)), while the second and third roll patterns with wavevectors $\pm\mathbf{k_2}$ and $\pm\mathbf{k_3}$ (Fig. 2(c2) and 2(c3)) contain a defect each. A standard demodulation technique is used here to study the structure of the defect [5]. As we know, the gray scale $A(\mathbf{x})$ of a nearly perfect hexagonal pattern can be written as:

$$A(\mathbf{x}) = \sum_{j=1}^{3} (\hat{A}_j(\mathbf{x}) e^{i\mathbf{k_j}\cdot\mathbf{x}} + c.c).$$

Here $\hat{A}_j(\mathbf{x})(j = 1, 2, 3)$ is the slow varying amplitude of one of the three superimposed roll patterns. These three complex amplitudes contain the essential information of the defect. To obtain $\hat{A}_j(\mathbf{x})$, we first shift the peak of $A(\mathbf{k})$ at $\mathbf{k_j}$ to the origin, and then do a low pass filtering (tanh window) [14] around the origin. The inverse Fourier transform of the filtered $A(\mathbf{k})$ gives us $\hat{A}_j(\mathbf{x})$. The phase of the $\hat{A}_j(\mathbf{x})$ is shown in Fig. 2(d1,d2,d3). No singularity is observed in the phase diagram of the first roll pattern (Fig. 2(d1)), while singularity of topological winding number $+/-1$ is shown at the core of the defect in the phase diagram of the second /third roll pattern (Fig. 2(d2)/Fig. 2(d3)). The definition of the phase winding number can be found in Ref. [9] and Ref. [13]. The modulus $|\hat{A}_j|^2$ of the complex amplitude demonstrates a minimum at the core of the defect for the second and the third roll patterns. Gray scale rendition of $|\hat{A}_2(\mathbf{x})|^2$ is shown in Fig. 2(e). The above shows that the structure of the PHD in a soap bubble raft presents similar characteristics as that observed in Rayleigh-Bénard convections [5,8].

The trajectory of the PHD is shown in Fig. 3 and it is extracted from a time series of 32 images. The x-y coordinates of the PHDs are determined by locating the positions of the singularities in the phase diagrams such as the one shown in Fig. 2(d2) using Global Lab Image software(Data Translation). As seen, the positions of the singularities are sharply defined in the phase diagrams(Fig. 2(d2,d3)). The error of each measured position is ± 1 pixel, which corresponds to $\pm 0.0084 cm$. The trajectory of the PHD is consistently straight in our experiments. The interesting finding here is that the isolated PHD always moves along the direction perpendicular to the wavevector of the nonsingular mode ($\mathbf{k_1}$ in our experiment). In other words, the PHD always prefer to climb along the defect free rolls. This is more clearly demonstrated by the arrows in Fig. 2(c1), in which the two ends of the arrows are determined by the locations of the PHDs of $5s$. apart. The motion of the defect in the second or the third roll pattern consists of both a glide and a climb motion. Movies of the defect motion can be seen at website http://mwu.phys.oxy.edu/soap-bubble/soap.html. The direction of the trajectory is also determined quantitatively using the slope of the trajectory from a linear fit to the data in Fig. 3. The angle between the trajectory and +x-axis is obtained to be -43.1^o. The direction of the wavevector $\mathbf{k_1}$ is determined using the location of the peak at $\mathbf{k_1}$ in Fig. 2(b), which gives us an angle of 48.4^o (between $\mathbf{k_1}$ and +x-axis). The angle between the direction of the trajectory and the wavevector $\mathbf{k_1}$ for this particular run is thus 91.5^o. Summarizing the 7 experimental runs, we obtain the angle between the wavevector $\mathbf{k_1}$ and the trajectory to be 90.8 ± 2.0^o.

To investigate the velocity of the PHD, we plot the distance that the PHD has travelled since its creation versus time (Fig. 4). The slope of that gives us the speed of the defect motion. In the several runs that we have, the speed of of the PHD is not a constant throughout the entire cell. It usually moves slower at the beginning (shown in Fig. 4), then it moves at a nearly contant speed in the central portion of the cell, and finally it moves faster when it is near the boundary. The velocity presented here is the velocity at the central portion of the cell. In this particular run, the velocity is obtained to be $0.0323 cm/s$. For the 7 runs that we have, the speed of PHD is in the range of 0.0139 - 0.0329 cm/s. The speed of the PHD is found to vary with the thickness of the fluid layer underneath the bubbles. The PHD moves faster when the layer is thicker. The current experimental setting does not allow us to change the layer thickness quantitatively, however, cautions have been taken to keep the layer thickness a constant from one run to the other. A new experimental apparatus is being contemplated to study such dependancy quantitatively.

A full theoretical explanation of the experimental results presented above is still lacking. Here, we would like to address a few issues that are pertinent to the problem. First of all, what is the driving force behind the PHD motion? Theoretical work on nonequilibrium systems [12] demonstrates that the driving force can be the Peach-Köhler force, which is due to the deviation of the wave vector from its optimal value. We compared the wave vector $\mathbf{k}_j$ of each of the roll pattern before and after the PHD moves out of the cell and found no differences in their values within experimental errors. This suggests that the driving force comes from other sources. Now, the fact that PHD leaves the bubble raft spontaneously suggest that there is a free energy associated with it, that work must be done to move the PHD into a perfect hexagonal pattern. This indicates that the driving force can be the potential force associated with the free energy of the system. We will show that this conjecture is consistent with our experimental results. A previous experiment on defect motion in a straight roll pattern in Rayleigh-Bénard convection [4]demonstrates that the defect always prefers climbing over gliding. Thus, it is conceivable to suggest that it takes more work to glide than to climb. Fig. 2(c1,c2,c3) shows that initially the roll patterns with wave vectors $\mathbf{k_2}$ and $\mathbf{k_3}$ are broken while rolls of $\mathbf{k_1}$ are defect free. In order to do minimum amount of work, the system naturally chooses to glide along the defect free rolls. The direction of the PHD is further finalized by the boundary. The PHD is found to always move towards the nearest boundary. The second issue concerns the speed of the PHD. The fact that the speed of PHD depends on the thickness of the fluid layer underneath the bubbles suggest that it is controlled by the viscous effect. If it is so, the magnitude of the speed should be $\sim l/t = \nu/l = 0.01cm/s$, which agrees well with our results. Here, $t = l^2/\nu$ is the time scale, $l = 4.0cm$ is the size of the cell and $\nu = 0.0401cm^2/s$ is the kinetic viscosity of the fluid. We further tested this hypothesis, and found that the PHD indeed moved faster in a smaller cell.

To summarize, we find that (1) an isolated PHD moves along the direction perpendicular to the wave vector of the nonsingular mode and towards the nearest boundary in a cell with free boundary; (2) an isolated PHD stays motionless in a cell with rigid boundary.

The authors would like to thank Professor Guenter Ahlers for insightful discussions on the subject. Wu would like to thank Dr. Tsimring on the various email communications, especially on the theoretical explanations of the results presented above. This work is supported by the Petroleum Research Fund (ACS-PRF# 32904-GB9) and the Research Corporation (CC4612).

FIGURES

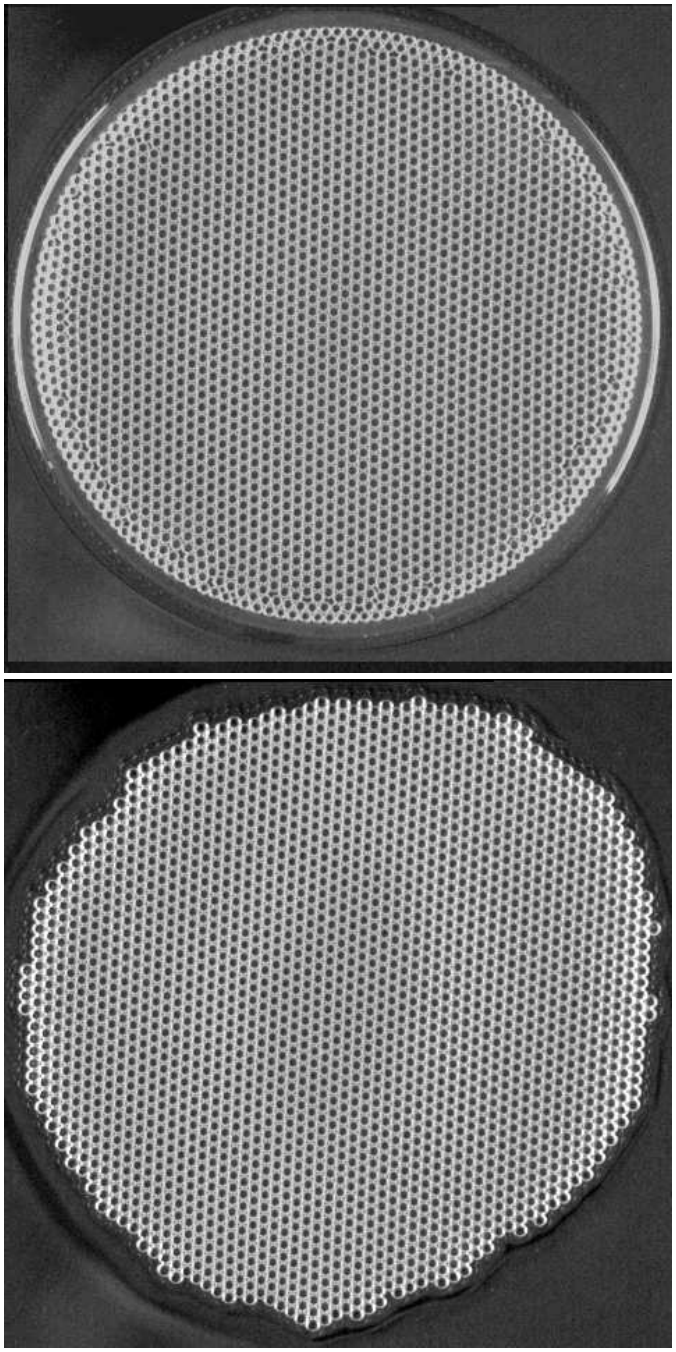

FIG. 1. Perfect hexagonal patterns formed by $0.108cm$ diameter soap bubbles. (a): The bubble raft is bounded with a $5.41cm$ diameter plastic ring. (b): The bubble raft has no boundary.

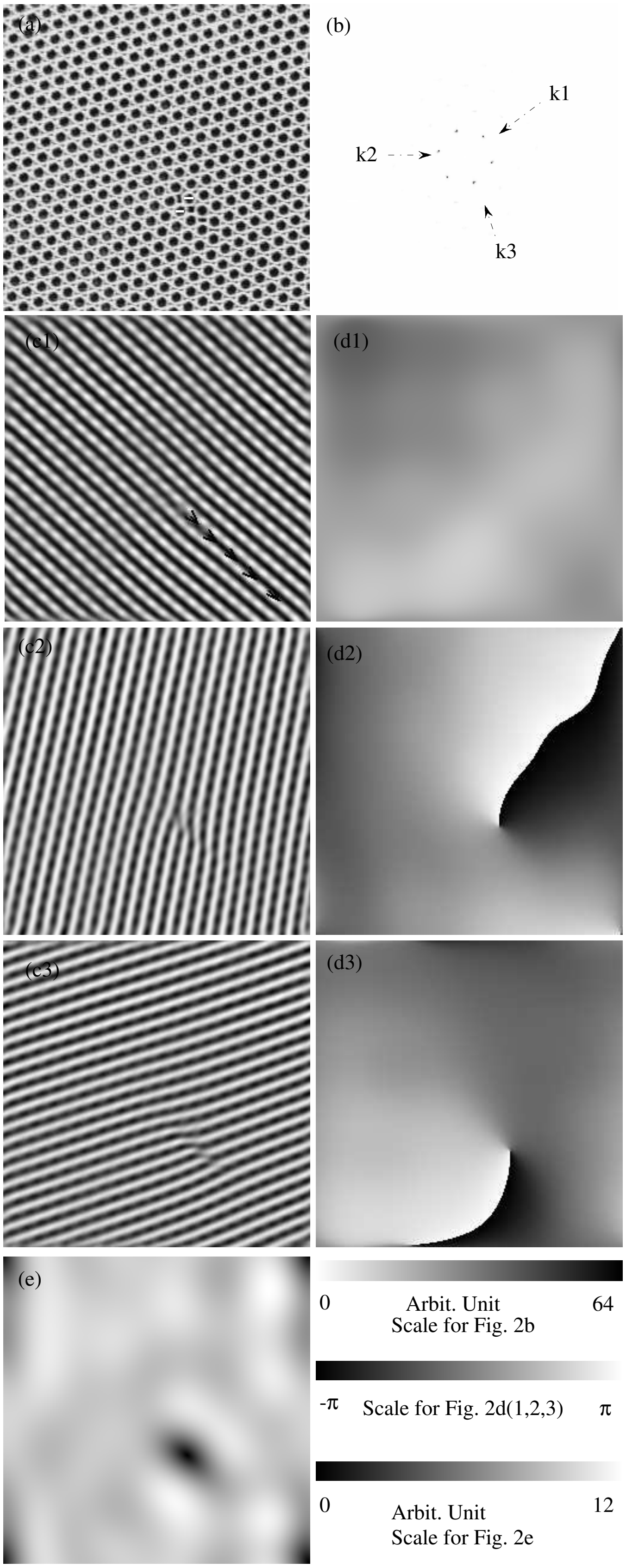
(a)
(b)
k1
k2
k3
(c1)
(d1)
(c2)
(d2)
(c3)
(d3)
(e)
0
Arbit. Unit
64
Scale for Fig. 2b
-π
Scale for Fig. 2d(1,2,3)
π
0
Arbit. Unit
12
Scale for Fig. 2e

FIG. 2. (a): Hexagonal pattern with an isolated PHD formed by soap bubbles of diameter 0.108cm. The pair of pentagonal and heptagonal cells are marked with two white bars. (b): Modulus $|A(\mathbf{k})|^2$ of the Fourier transform of the hexagonal pattern shown in Fig. 2(a). Linear gray scale is shown at the lower right corner of Fig. 2. Note the inverse gray scale. (c1,c2,c3): Three roll patterns with wavevectors $\mathbf{k_1}, \mathbf{k_2}$ and $\mathbf{k_3}$. The arrows in Fig. (c1) indicates the direction and trajectory of the PHD. The two ends of each arrow are determined by the locations of the defects of 5s. apart. (d1,d2,d3): Gray scale renditions of the phases of the complex amplitudes $\hat{A}_j(\mathbf{x}) (j = 1, 2, 3)$. Linear gray scale is shown at the bottom. (e): Gray scale rendition of the square root of $|\hat{A}_2(\mathbf{x})|^2$. Linear gray scale is shown on the right side of the image.

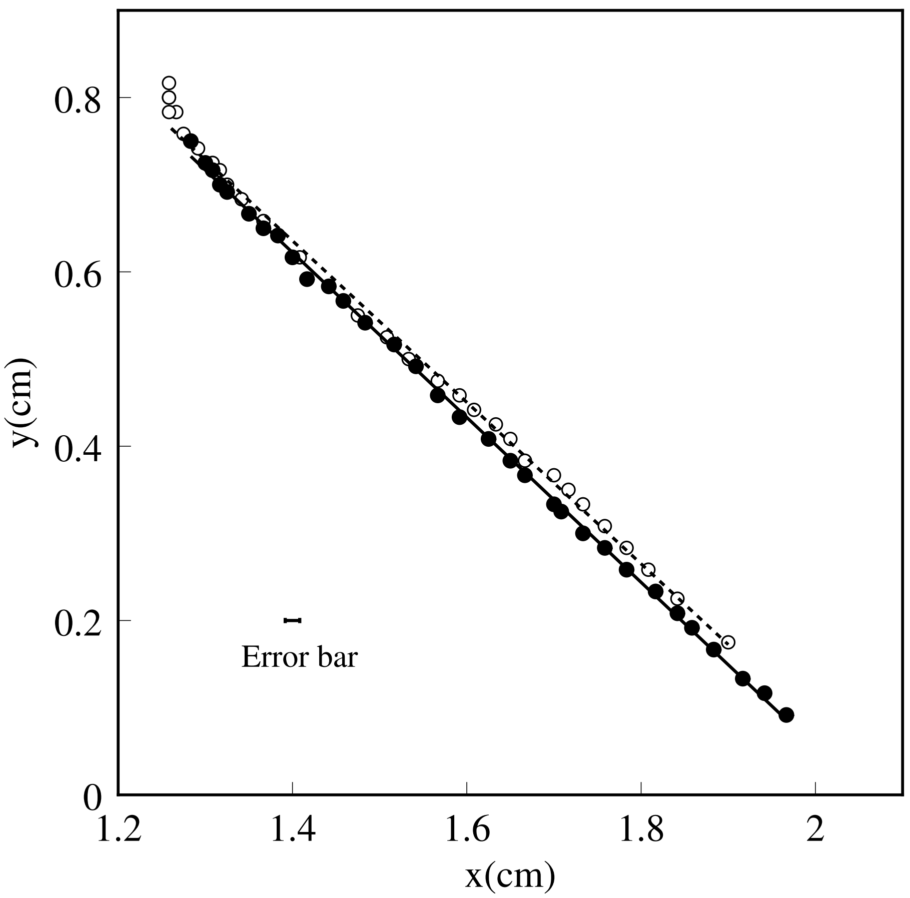

FIG. 3. Trajectory of the PHD. The origin (0,0) of the plot corresponds to the lower left corner of the image. x and y axis are the (x,y) coordinates of the PHD. $\circ/\bullet$: Data points determined using phase diagram of the roll pattern with wavevector $\mathbf{k_2}/\mathbf{k_3}$. Dashed/Solid line is obtained from the linear fit to $\circ/\bullet$ data points.

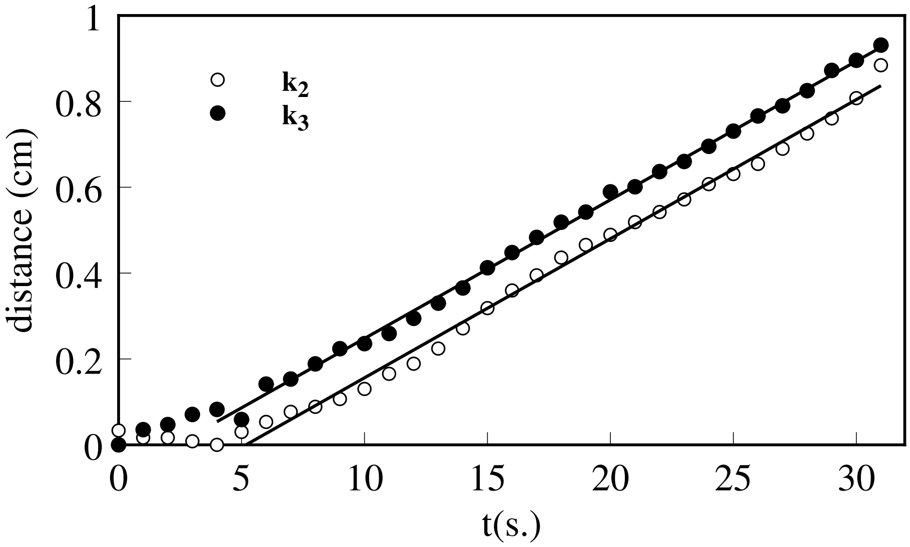

FIG. 4. Distance of the PHD from its starting point versus time. ∘/•: Data points determined using the phase diagram of the roll pattern with wavevector $\mathbf{k_2}/\mathbf{k_3}$. Solid lines are obtained from linear fits to the experimental data.

REFERENCES

[1] L. Bragg, J. Sci. Instrum., **19**, 148(1942).

[2] L. Bragg and J. F. Nye, Proceedings of the Royal Society of London, **190**, 474(1947).

[3] M. M. Nicolson, Proceedings of the Cambridge Philosophical Society, **45**, part 2, 288(1948).

[4] V. Croquette, Contemp. Phys., **30**, 153(1989).

[5] S. Ciliberto, P. Coullet, J. Lega, E. Pampaloni, and C. Perez-Garcia, Phys. Rev. Lett., **65**, 2370(1990).

[6] S. Ciliberto, E. Pampaloni, and C. Perez-Garcia, J. Stat. Phys., **64**, 1045(1991).

[7] J. de Bruyn, E. Bodenschatz, S. Morris, S. Trainoff, Y. Hou, D. Cannell and G. Ahlers, Rev. Sci. Inst., **67**, 2043(1996).

[8] E. Bodenschatz, W. Pesch and G. Ahlers, Annu. Rev. Fluid Mech., to be published.

[9] M. Cross, P. Hohenberg, Rev. Mod. Phys., **65**, 898-922(1993).

[10] L. M. Pismen and A. A. Nepomnyashchy, Europhysics Lett., **24**, 461(1993).

[11] M. I. Rabinovich and L. S. Tsimring, Phys. Rev. E., **49**, R35(1994).

[12] Lev S. Tsimring, Phys. Rev. Lett., **74**, 4201(1995).

[13] Lev S. Tsimring, Physica D, **89**, 368(1996).

[14] A function $0.25(tanh\frac{r+4}{10}+1)(tanh\frac{4-r}{10}+1)$ is used to multiply $A(\mathbf{k})$, where r is the distance to the peak $\mathbf{k}_j$. The function has a hat shape that centers around $r=0$, the top width is 4 and bottom width is 10.